Quadratic Thermal Convection in Magneto-Casson Fluid Flow Induced by Stretchy Material with Tiny Particles and Viscous Dissipation Effects

E. O. Fatunmbi [a*] and O. A. Agbolade [a]

[a] *Department of Mathematics and Statistics, Federal Polytechnic, Ilaro, Nigeria.*

Authors' contributions

This work was carried out in collaboration between both authors. Both authors read and approved the final manuscript.

Original Research Article

ABSTRACT

This investigation is based on the phenomenon of quadratic thermal convection in Magneto-Casson fluid flow induced by stretchy material with tiny particles and viscous dissipation effects. The study aims to understand and optimize the complex behaviour of fluid flow and heat transfer in this system, which has significant implications for engineering and industrial applications. The Magneto-Casson fluid, characterized by its non-Newtonian behaviour and yield stress, interacts with stretchy material and tiny particles, introducing unique flow characteristics and thermal properties. Viscous dissipation, resulting from internal friction, further influences the convective heat transfer process. Mathematical models are developed and solved by employing a numerical technique through the Runge-Kutta Fehlberg scheme coupled with the shooting method to investigate these phenomena comprehensively. The results are deliberated using several graphs on the dimensionless profiles. The results showed that there is a decline in the momentum boundary film as the magnetic field improves due to the effect of the Lorentz force. Also, an increase in the Casson fluid term raises the viscosity and thereby resists the fluid motion.

_____

Corresponding author: E-mail: ephesus.fatunmbi@federalpolyilaro.edu.ng;

1. INTRODUCTION

Non-Newtonian fluids are indispensable in all areas of human endeavour due to their broad applications, including industrial and engineering processes. Crude oil drilling, food processing, bio-engineering, polymer processing, and the like are some of the areas of application for these types of fluids. Several constitutive models for non-Newtonian fluids have been derived since it is difficult to describe all the non-Newtonian fluid attributes using a single model Gbadeyan et al. [1]; Fatunmbi and Okoya [2]; Rajput et al. [3]; Khan et al. [4]; Fatunmbi et al. [5]. The Casson fluid model is one of the non-Newtonian fluid models that captures the description of fluids with yield stress. This kind of fluid characterizes an elastic solid when the shear stress is low but demonstrates the character of a Newtonian fluid at higher rates of shear stress. In addition it exhibits a shear-thinning nature at a point of no shear, whereas at an infinite rate of shear, there are infinite viscosity attributes. Examples of this kind of fluid include honey, animal blood, tomato sauce, and the like [6]. The derivation of this model was initiated by Casson [7], while an extensive study has been carried out by various researchers with attention placed on different parameters, geometry, and methods. For instance, the flow of a Casson fluid across a boundary layer coupled with heat transmission was reported by Reza et al. [8] over a porous, elongated sheet that stretches non-linearly the flow direction. Qing et al. [9] engaged the successive linearization method coupled with the Chebyshev spectral collocation technique to examine the Casson fluid motion over a porous extending device, capturing the impact of nonlinear radiation and chemical reactions. In their report, it was noted that the Casson fluid parameter accelerated the motion, whereas the opposite trend occurred with the magnetic field term. Sohail et al. [10] discussed the significance of radiation and Joulean heating on Casson fluid flow over a flat, three-dimensional, extending plate with temperature-dependent thermal conductivity. Meanwhile, Omotola and Fatunmbi [11] consider such a kind of subject on a non-linearly extending material having the influence of viscous dissipation in the thermal vicinity. The analysis revealed that heat transmission increased with growth in the Eckert number and radiation term.

Hydromagnetic flow is now popular owing to its various practical uses in the fields of engineering, nuclear reactors, power plants, the crude oil industry, and so on. The suspension of nanoparticles in orthodox fluids like water, oil, etc. produces a new class of fluids known as nanofluids, which have the tendency to boost the thermal properties and encourage the transfer of heat in various devices. The combination of this new class of fluids with magnetic fields has been found useful in diverse areas such as transportation industries, drug and pharmaceutical industries, etc. Thus, incorporating a magnetic field into the flow of Casson fluids with tiny particles allows for tailoring heat transfer characteristics that propel better control in industrial operations and lead to increased productivity and cost-effectiveness. Rashidi et al. [12] evaluated the incompressible buoyancy-driven flow of a nanofluid under the influence of a magnetic field and thermal radiation over an elongated material in this manner. In an extension, Babu and Sandeep [13] employed a numerical method to calculate hydromagnetic nanofluid motion around a stagnation point featuring motile microorganisms when the viscosity is non-constant. It was reported that the magnetic field and thermophoresis terms caused a significant growth in the thermal field. Fatunmbi et al. [14] assessed the transport of a reactive Eyring-Powell fluid consisting of tiny particles over a Riga sheet with nonuniform heat conductivity and thermophoresis impact. The authors stated that thermophoresis and Brownian diffusion raised the heat profile and the thermal boundary structure. Mishra et al. [15] looked at MHD nanofluid flow with heat and mass transfer effects over a two-dimensional material device that stretches in a nonlinear way with thermal radiation and Joulean heating effects. Their analysis reveals that the skin friction coefficient is a decreasing function of the magnetic field term, whereas the heat transfer phenomenon is enhanced in the presence of the magnetic field and Brownian motion parameters.

Mondal et al. [16] discussed the impact of fluid variable viscosity on hydromagnetic dusty nanofluid over a permeable stretching plate, which is influenced by thermal radiation and entropy generation. The authors engaged the spectral quasi-linearization method to obtain the solutions to the governing equation. Kumar et al. [17] developed a numerical model to investigate

the transport of hydromagnetic fluid containing tiny particles over an infinite vertical device when there is the impact of thermal radiation together with viscous dissipation. Convective heat transfer has an impact on many fields of science and technology, including the dynamics of geophysical fluids, the cooling of electronic devices, and the design of thermal management systems. In various industrial and manufacturing processes, it is important to control heat transfer for efficient operations. Hence, studying convective heat transfer properties over different configurations in complex fluid systems will adequately inform engineers on how to enhance process parameters, reduce energy consumption, and boost product quality. Fatunmbi et al. [18] engaged convective heating boundary and uniform surface temperature boundary conditions to investigate the heat transfer mechanism of a steady, magneto-micropolar fluid consisting of minute nanoparticles over a vertically extending sheet in porous media. The report shows that there is an improvement in the mechanism of heat transfer when the radiation term is raised.

When there is a high temperature distribution in the flow region, the use of nonlinear thermal convection becomes useful for effective prediction of the flow regime. In this view, Thriveni and Mahanthesh [19] examined the flow of free convection using nonlinear density variation over a uniform temperature distribution at the wall. Fatunmbi and Okoya [20] looked into the case of a Casson nanofluid with mixed convective flow and variable thermophysical properties when there is ohmic heating and a heat source nearby. Other notable works have been done with this concept (Kameswaran et al. [21]; Jha and Gwandu [22]; RamReddy [23]; Sajjian et al. [24]; Mahanthesh [25].

In view of the above literature coupled with the crucial application of the current investigation in industrial and engineering processes as discussed above, the aim of the current work is to numerically examine quadratic thermal convection flow in a magneto-Casson fluid consisting of tiny particles. The flow is induced by a stretchy device with transpiration velocity, viscous dissipation, thermal radiation, and a prescribed surface temperature. A mathematical model is developed in partial differential equation form and transformed into ordinary derivatives, which are then solved via a numerical technique. Graphs and Tables are constructed to determine the impact of each parameter on the flow region.

The novelty in the current work is in the incorporation of the quadratic Boussinesq approximation in the momentum equation, coupled with the use of the Prescribed surface temperature in the thermal boundary condition. This research is applicable not only for electronic cooling and manufacturing but also in geophysical work. The findings in this study will further enhance the knowledge of thermal convection, which ultimately will foster technological advancements and sustainable solutions.

2. FORMULATION OF THE PROBLEM

For the derivation of the governing equations that physically describe the present investigation, it is assumed that there is an incompressible and steady motion of a hydromagnetic Casson fluid flow with tiny particles, which is occasioned by a stretchy material device. The material device is configured as a two-dimensional plate that extends vertically in x direction while y axis is normal to it, as portrayed in Fig. 1. A magnetic field is imposed externally in the transverse direction of the flow regime, but there is no consideration for the induced one. In the thermal vicinity, there is the presence of thermal radiation, which is simplified by the Roseland approximation. The momentum equation considers the impact of linear and quadratic thermal convection, while thermal heating is taken to be of a prescribed wall temperature with a power index.
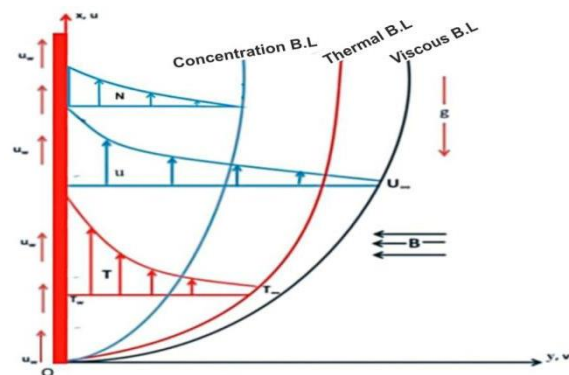

Fig. 1. The flow geometry

2.1 Equations Governing the Problem

Due to the above-mentioned assumptions the equations describing the current problem are specified as follows:

$$\frac{\partial u_1}{\partial x} = -\frac{\partial u_2}{\partial y}, \tag{1}$$

$$\rho_f\left(u_1\frac{\partial u_1}{\partial x} + u_2\frac{\partial u_1}{\partial y}\right) = g^\star[\alpha_1(T - T_\infty) + \alpha_2(T - T_\infty)^2 + \alpha_3(\xi - \xi_\infty)] + \left(1 + \frac{1}{\gamma}\right)\frac{\partial^2 y}{\partial y^2} - \sigma B_0^2 u_1 \tag{2}$$

$$u_1\frac{\partial T}{\partial x} + u_2\frac{\partial T}{\partial y} - \frac{k_f}{(\rho c_p)_f}\frac{\partial^2 T}{\partial y^2} = \beta\left[\frac{D_t}{T_\infty}\left(\frac{\partial T}{\partial y}\right)^2 + D\left(\frac{\partial T}{\partial y}\frac{\partial \xi}{\partial y}\right)\right] + \left(1 + \frac{1}{\gamma}\right)\frac{1}{(\rho c_p)_f}\left(\frac{\partial u_1}{\partial y}\right)^2$$

$$+ \frac{\sigma B_0^2}{(\rho c_p)_f}u_1^2 + \frac{16\sigma^\star T_\infty}{3q(\rho c_p)_f}\frac{\partial^2 T}{\partial y^2}, \tag{3}$$

$$u_1\frac{\partial \xi}{\partial x} + u_2\frac{\partial \xi}{\partial y} = D\frac{\partial^2 \xi}{\partial y^2} + \frac{D_t}{T_\infty}\left(\frac{\partial^2 T}{\partial y^2}\right) - k_r(\xi - \xi_\infty). \tag{4}$$

The wall constraints suitable for these equations are:

$$u_1(x,0) = bx, u_2(x,0) = Zw, T(x,0) = T_w = (Hx^r + T_\infty), \xi = \xi_w \ at \ y = 0$$
$$u_1 \to \infty, T \to \infty, \xi \to \infty \ as \ y \ \to \infty. \tag{5}$$

The symbols used in the above governing equations are described as follows: u_1, u_2 components of velocity along x, y directions, $\gamma, v_f, \rho_f, \xi, g^\star, b, Zw, H, kr, \sigma, (\rho c_p)_f, a_1$ and a_2 respectively connotes Casson fluid term, kinematic viscosity, fluid density, concentration, gravitational acceleration, stretching constant, wall transpiration velocity, temperature constant, chemical reaction rate, electrical conductivity, heat capacity of the fluid, linear thermal

expansion, nonlinear thermal expansion. Further, D symbolizes Brownian diffusion coefficient, D_t connotes thermophoretic diffusion and μ_f defines the dynamic viscosity. The original equations controlling the motion are transmuted into ordinary derivatives via similarity quantities listed under while some dimensionless parameters are also incorporated into the governing equations as follows:

$$\eta = y\sqrt{\frac{b}{v_f}}, u_1 = bx\frac{df}{d\eta}, u_2 = -\sqrt{bv_f}f(\eta), \theta = \frac{T - T_2}{T_1 - T_2}, \phi = \frac{\xi - \xi_2}{\xi_1 - \xi_2}, PR = \frac{\mu_f c_p}{k_f}, M = \frac{\sigma B_0^2}{c\rho_f},$$

$$NR = \frac{16\sigma^\star T_\infty^3}{3k^\star k_\infty}, EC = \frac{u_w^2}{c_p(T_1 - T_2)}, \lambda = \frac{Gr_x}{Re_x^2}, SC = \frac{v_f}{D}, \gamma_r = \frac{\xi_r}{b}, NT = \frac{D_t\beta(T_1 - T_2)}{T_2 v_f}, \tag{6}$$

$$NB = \frac{D\beta(\xi_1 - \xi_2)}{v_f}, G = \frac{a_2(T_1 - T_2)}{a_1}, Gr_x = \frac{g^\star a_1(T_1 - T_2)x^3}{v^2}, FW = -\frac{Zw}{\sqrt{bv_f}}, Gc = \frac{g^\star a_3(\xi_1 - \xi_2)}{b^2 x}.$$

Using equation (6) leads to the validity of equation (1) while equations (2,3,4) together with the boundary conditions (5) simply becomes:

$$\left(1 + \frac{1}{\gamma}\right)\frac{d^3 f}{d\eta^3} + \frac{df}{d\eta}\frac{d^2 f}{d\eta^2} - \left(\frac{df}{d\eta}\right)^2 - M\frac{df}{d\eta} + \lambda[\theta(1 + G\theta)] + Gc\phi = 0, \tag{7}$$

$$(1 + NR)\frac{d^2\theta}{d\eta^2} + PRECM\left(\frac{df}{d\eta}\right)^2 + PR\left(f\frac{df}{d\eta} - r\frac{d\theta}{d\eta} + EC\left(1 + \frac{1}{\gamma}\right)\left(\frac{d^2 f}{d\eta^2}\right)^2\right) + PR(NT\left(\frac{d\theta}{d\eta}\right)^2 +$$
$$NB\left(\frac{d\theta}{d\eta}\right)\left(\frac{d\phi}{d\eta}\right) = 0 \tag{8}$$

$$\frac{d^2\phi}{d\eta^2} + SCf\frac{d\phi}{d\eta} - SC\gamma_r\phi + \frac{NT}{NB}\frac{d^2\theta}{d\eta^2} = 0. \qquad (9)$$

Further, the wall constraints transformed to:

$$(10)$$

$$at\ \eta = 0: \frac{df}{d\eta} = 1, f(\eta) = Fw, \theta(\eta) = 1, \phi(\eta) = 1$$

$$as\ \eta \to \infty: \frac{df}{d\eta} = 0, \theta(\eta) = 0, \phi(\eta) = 0.$$

The preceding equations (7-10) features γ as the Casson material term, λ as the mixed convection term, PR as the Prandtl number while M as the magnetic field term, Gc as solutal term, RD as the radiation term whereas EC as the Eckert number, G as the nonlinear thermal convection term, SC as the Schmidt number, NT as thermophoresis term, NB as the Brownian motion, FW is the transpiration velocity, γ_r as the reaction term, NR is the radiation parameter, λ mixed convection parameter, NT is the thermophoresis term and Nb indicates the Brownian motion sequentially. Further, the engineering interest in the current work are described as the wall drag factor (W_{Fx}), this depicts friction at the boundary occasioned the fluid and the stretching plate. The other important parameters are the Nusselt number N_x which shows the amount of surface heat transfer and the Sherwood number (SH_x). The underlisted equations respectively show these parameters.

$$(11)$$

$$W_{Fx} = \frac{w}{\rho_f U_w^2}, N_x = \frac{xq_w}{k_f(T_1 - T_2)}, SH_x = \frac{xq_m}{D_B(\xi_1 - \xi_2)}.$$

The dimensionless forms of these parameters are

$$(12)$$

$$W_{Fx} = \left(1 + \frac{1}{\gamma}\right)Re_x^{-1/2}\frac{d^2f}{d\eta^2}\ at\ \eta = 0,$$

$$(13)$$

$$N_x = -(1 + NR)Re_x^{1/2}\frac{d\theta}{d\eta}, SH_x = -Re_x^{1/2}\frac{d\phi}{d\eta}\ at\ \eta = 0.$$

3. PROBLEM SOLUTION TECHNIQUE

Due to the extreme non-linearity of the governing equations (9,10,11), when subjected to the wall conditions (12), a numerical solution is sought by employing Runge-Kutta-Fehlberg in conjunction with shooting techniques. Due to its precision and consistency, this approach works well for nonlinear ordinary differential equations. Several authors have applied this technique Ali [26]; Attili and Syam [27], Fatunmbi and Okoya [2]; Mahanthesh et al. [28]. The codes developed are executed in the Maple software using the Runge-Kutta-Fehlberg scheme. By comparing the calculated values of the Nusselt number to those found in previous studies that considered the same range of values for the Prandtl number PR and the temperature exponent a, we can be confident in the accuracy of the results obtained. According to Table 1, the present results agree well with the prior study. The range of values for the embedded parameter in the current study aretaken $NR = 0.3, M = 0.5, NT = 0.5, \gamma = 0.3, \gamma_r = 0.2, a = 0.5, SC = 0.62, G = 0.5, Gc = 0.3, \lambda = 0.2, FW = 0.2, EC = 0.2, NT = NB = 0.5$. These values are used in the computation except otherwise stated in the figures. The developed codes for the results have been verified with previously published data for the Nusselt number when the temperature exponent and Prandtl number vary in magnitude. This comparison is collated in Table 1, which shows an excellent relationship. The developed codes for the results have been verified with previously published data for the Nusselt number N_x when the temperature exponent a and Prandtl number Pr vary in magnitude. This comparison is collated in Table 1, which shows an excellent relationship.

4. DISCUSSION OF OUTCOMES

The significant contributions of the embedded parameters are depicted in graphs and tables under this section, along with appropriate discussions of their trends on the dimensionless quantities.

The outcome of increasing M on the3 flow field is portrayed in Fig. 2. It is of interest to note that there is a deceleration in the speed of the Casson fluid as M increases. In this view, the flow of the fluid can be controlled by adjusting the magnitudes of M. The interaction between the electro-conducting Casson fluid and the magnetic field produces Lorentz force, which is draglike in nature. At such a point, resistance is introduced in the Casson fluid motion as there is an increase in M. However, there is an opposite trend in the thermal field with a rise in M as demonstrated in Fig. 3. The thickness of

the boundary layer expands, and there is a higher temperature distribution as M uplifts. The escalation in the thermal field is caused primarily by the friction that occurs because of the flow resistance as a result of the Lorentz force.
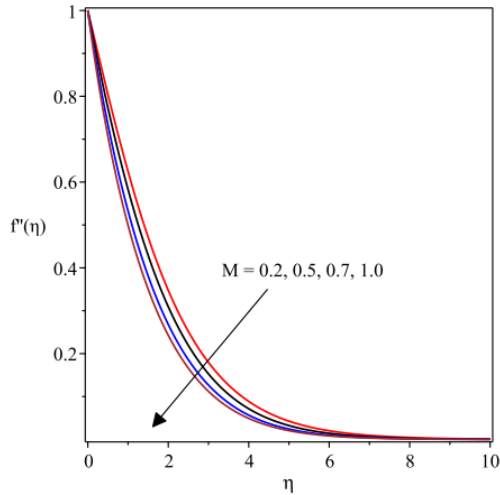

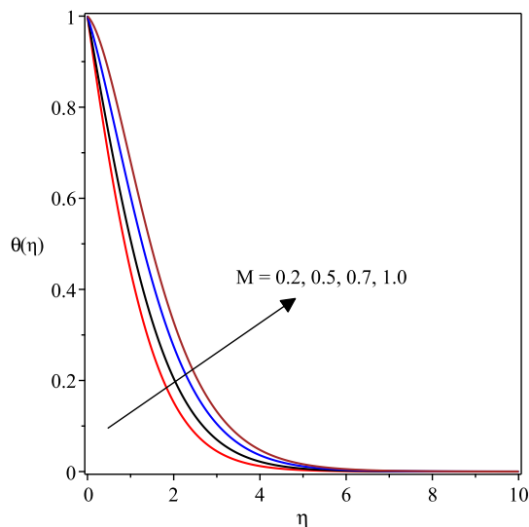**Fig. 2. Magnetic field term effect on** $f'(\eta)$

Fig. 3. Magnetic field term effect on $\theta(\eta)$

The Casson parameter γ causes the velocity profiles to shrink together with the hydrodynamic boundary layer, as found in Fig. 4. The trend is due to the fact that as γ increases in value, the fluid viscosity rises, and as such, drag is introduced in the flow field, leading to a decline in motion. Meanwhile, the mixed convection term λ behaves otherwise on the velocity profile, as noted in Fig. 5. When λ is raised, the fluid's

hydrodynamic structure is pushed upward, which in turn accelerates the transport field. Moreover, with an increase in λ, the buoyancy force is increased, and the viscous force is suppressed, resulting in less resistance to the motion of the Casson fluid.
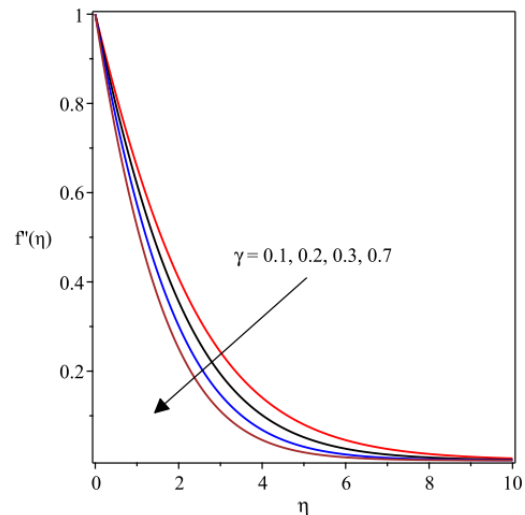

Fig. 4 Casson parameter γ **effect on** $f'(\eta)$

The graph displayed in Fig. 6 elucidates the trend of the thermal field with variations that occur in the value of Eckert's term EC. Clearly, advancing EC raises the thermal profile $\theta(\eta)$ as portrayed in this figure. The trend can be attributed to the friction in the fluid particles due to viscous dissipation. More heat is generated due to this friction and the stretching material; thereby, temperature distribution increases in the thermal vicinity. In the same manner, there is an expansion in the thermal structure as NR increases, as demonstrated in Fig. 7. The mean absorption coefficient depreciates as NR increases, and consequently, there is a spread in the temperature as more heat is generated. Also, the heat profile is improved because of the direct correlation between heat conduction and expansion in NR.

Fig. 8 depicts how the thermal structure and heat dispersion are lowered due to the temperature exponent term a .. On the other hand, the concentration field rises significantly due to higher values of NT as plotted in Fig. 9. In this case, the thermal movement of the tiny particles suspended in the Casson base fluid boosts the concentration profile and thereby raises the distribution. Thermophoretic force propels an

increase in the thermal region because of the temperature gradient. On the contrary, the reaction of the Brownian diffusion term NB on the concentration profile is found to be of decreasing nature, as plotted in Fig. 10. There is a decline in the thermal film layer with an improvement in the values of PR as depicted in Fig. 11, and as such, the heat impact drops significantly in the flow region. More so, the thermal diffusivity depreciated, whereas the momentum diffusivity behaved otherwise as PR rose in value. Such a behaviour causes the thermal field to depreciate, and less heat is distributed.

In Table 2, it is noted that growing values of the Casson term γ and that of the magnetic field term lead to higher friction at the wall as the skin friction coefficient FW_x is raised due to these parameters. Contrarily, as the values of the nonlinear thermal convection and mixed convection terms improved, there was a reduction in the frictional factor. Likewise, there is a significant improvement in the heat transfer due to higher values of G and λ as found in this table. The Casson parameters γ and M however, lessen the rate of heat transfer across the device, as noted in Table 2.
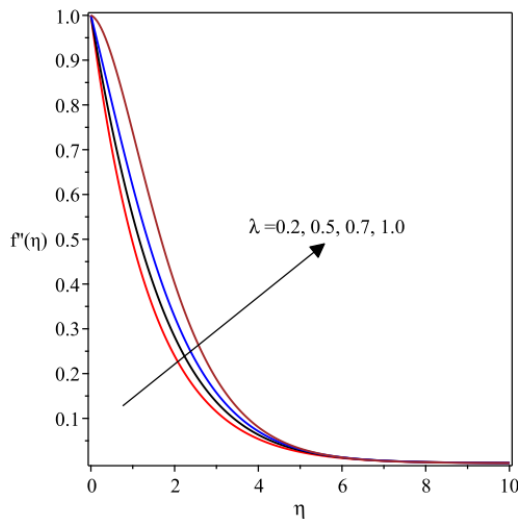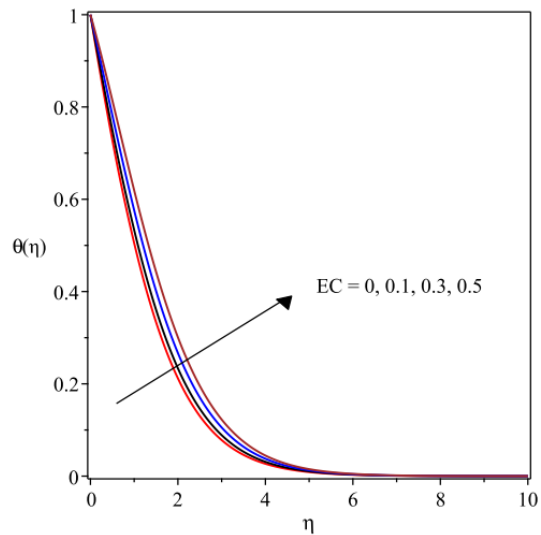

Fig. 5 Mixed convection λimpact on $f'(\eta)$

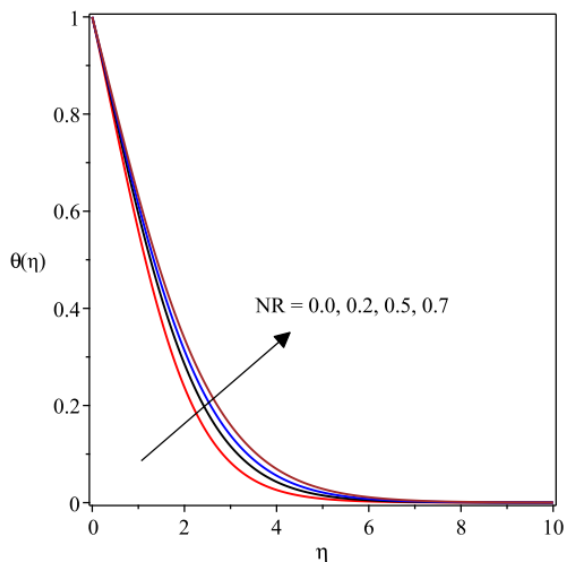**Fig. 6. Thermal profile for values of EC**
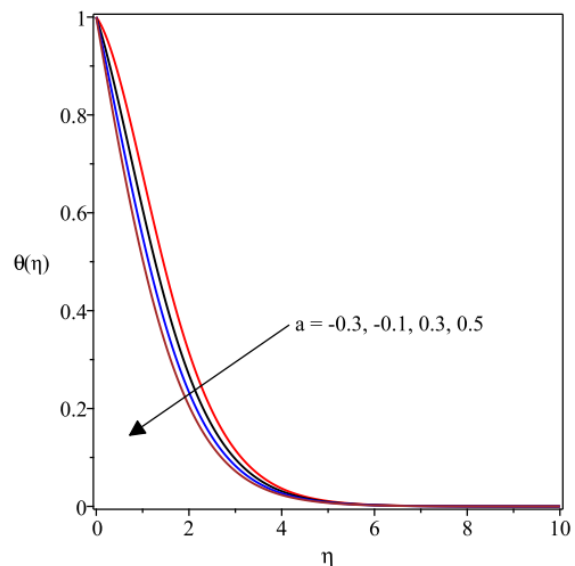

Fig. 7. Thermal distribution for NR

Fig. 8. Thermal profile for values a

Table 1. Values of N_x compared to what has been reported in the literature when the temperature exponent a and PR vary in the thermal

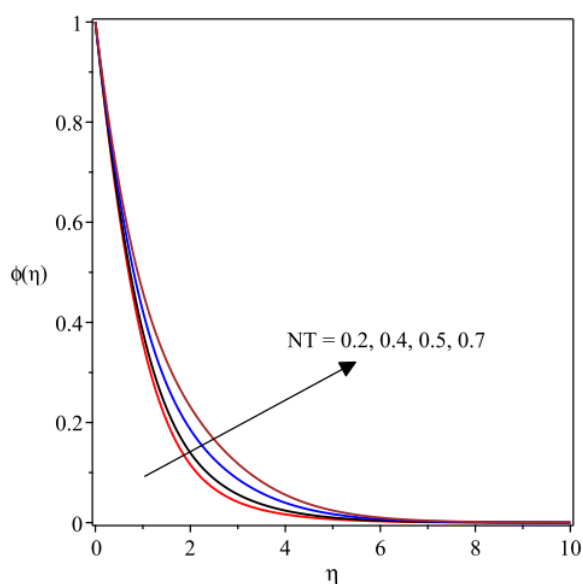| a	Grubka and Bobba [29]		current work	
	$PR = 0.72$	$PR = 1.0$	$PR = 0.72$	$PR = 1.0$
- 2.0	0.7200	1.0000	0.72069	0.99945
- 1.0	0.0000	0.0000	-0.00110	0.00012
0.0	-0.4631	-0.5820	-0.46359	-0.58201
1.0	-0.8086	-1.0000	-0.80883	-1.00001
2.0	-1.0885	-1.3333	-1.08862	-1.33333
3.0	-1.3270	-1.6154	-1.32707	-1.61538

Fig. 9. Concentration profile for values of NT
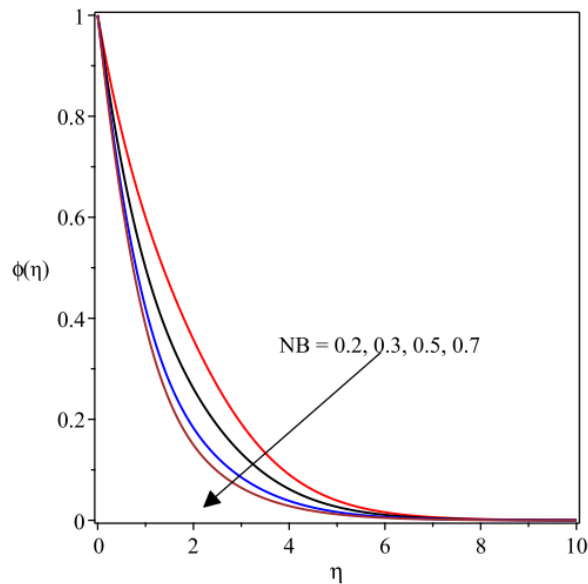

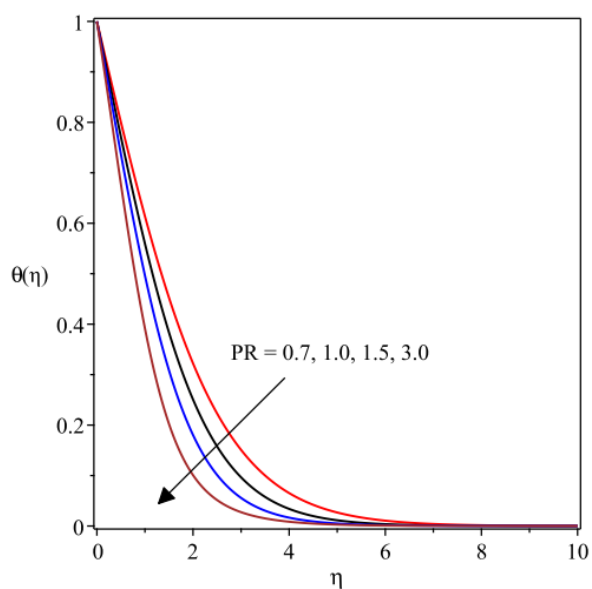**Fig. 10. Concentration field for NB**

Fig. 11. Thermal profile for increasing values of PR

Table 2. Values of FW_x and N_x for variations in γ, G, λ and M

γ	G	λ	M	FW_x	N_x
0.1	0.3	0.8	0.5	0.2505354	0.2160907
0.2				0.3076147	0.1920101
0.5				0.3618944	0.2290604
0.3	0.1			0.3649240	0.2188121
	0.3			0.3401395	0.2247617
	0.5			0.3156412	0.2302968
	0.0	0.2		0.5066346	0.1601615
		0.4		0.4740227	0.1753359
		0.6		0.4190308	0.2003560
		0.8	0.0	0.2568162	0.4337022
			0.3	0.3083807	0.3102189
			0.7	0.3701611	0.1366536

5. CONCLUSION

The current study looked at the effects of various parameters on the movement of hydromagnetic Casson fluid due to stretchy material with viscous dissipation in the thermal field. Linear and quadratic convection are incorporated in the momentum equation, while the impact of the temperature exponent is checked in the thermal boundary vicinity. Also, the Casson fluid is mixed with tiny particles, and the concentration field is used to figure out how the thermophoresis and the random movement of the particles affect the field. The developed partial derivatives describing the physical phenomenon are transformed into ordinary derivatives and solved with the Runge-Kutta Fehlberg method associated with the shooting technique. The accuracy of the developed codes is verified by comparing the obtained data with related ones previously published and found to be highly correlated. The study reveals that:

- There is a decline in the momentum boundary film as the magnetic field improves due to the effect of the Lorentz force. Also, an increase in the Casson fluid term raises the viscosity and thereby resists the fluid motion.
- There is an expansion in the thermal structure and a rise in the heat distribution as the thermal radiation, magnetic field, and Eckert number terms improve in magnitude. However, the temperature exponent and Prandtl number decreased the thermal field.
- The concentration profile witnesses a rise in the profile with growth in the thermophoresis term, but a decrease occurs in its profiles as the Brownian diffusion improves.
- The heat transfer can be improved by the higher magnitude of the mixed convection and nonlinear thermal convection terms, whereas the reduction in the skin friction factor can be achieved by these terms.

COMPETING INTERESTS

Authors have declared that no competing interests exist.

REFERENCES

1. Gbadeyan JA, Titiloye EO, Adeosun AT. Effect of variable thermal conductivity and viscosity on casson nanofluid flow with convective heating and velocity slip, Heliyon. 2020;6:e03076.
2. Fatunmbi EO, Okoya SS. Heat transfer in boundary layer magneto-micropolar fluids with temperature-dependent material properties over a stretching sheet. Advances in Materials Science and Engineering. 2020:1-11.
   DOI: 10.1155/2020/5734979
3. Rajput GR, Shamshuddin MD, Salawu SO. Thermo solutal convective non-newtonian radiative casson fluid transport in a vertical plate propagated by arrhenius kinetics with heat source/sink. Heat Transfer. 2020;20:10.
4. Khan MI, Waqas M, Hayat T, Alsaedi A. Colloidal study of Casson fluid with homogeneous-heterogeneous reactions. Colloid Interface Sci., 2017;498, 850.
5. Fatunmbi EO, Adeosun AT, Salawu SO. Entropy analysis of nonlinear radiative

casson nanofluid transport over an electromagnetic actuator with temperature-dependent properties. Partial Differential Equations in Applied Mathematics. 2021;4:100152.

6. Mukhopadhyay S, Bhattacharyya PRK. Casson fluid flow over an unsteady stretching surface. Ain Shams Eng. J. 2014;4(4):933-938.

7. Casson N. Rheology of Disperse Systems. Pergamon. 1959:84-02.

8. Reza M, Chahal R, Sharma N. Radiation effect on MHD Casson fluid flow over a power-law stretching sheet with chemical reaction. World Academy of Science, Engineering and Technology, International Journal of Chemical, Molecular, Nuclear, Materials and Metallurgical Engineering. 2016;10(5):566-571.

9. Qing J, Bhatti MM, Abbas MA, Rashidi MM, Ali ME. Entropy generation on MHD casson nanofluid flow over a porous stretching/shrinking surface, Entropy. 2016;18:1-14.

10. Sohail M, Shah Z, Tassaddiq A, Kumam P, Roy P. Entropy generation in MHD casson fuid fow with variable heat conductance and thermal conductivity over non-linear bi-directional stretching surface, Scientific. 2020;10:1-16.
DOI: 10.1038/s41598-020-69411-2

11. Omotola OE, Fatunmbi EO. Dynamics of multiple slip and thermal radiation on hydromagnetic casson nanofluid flow over a nonlinear porous stretchable surface. Physical Science International Journal. 2021;25(4):1-14.

12. Rashidi MM, Ganesh NV, Abdul AK, Ganga HB. Buoyancy effect on MHD flow of nanofluid over a stretching sheet in the presence of thermal radiation. Journal of Molecular Liquids. 2014;198:234-238.

13. Babu MJ, Sandeep N. Effect of nonlinear thermal radiation on non-aligned bio-convective stagnation point flow of a magnetic-nanofluid over a stretching sheet. Alexandria Engineering Journal. 2016;55(3):1931-1939.

14. Fatunmbi EO, Adeosun AT, Salawu SO. Irreversibility Analysis for Eyringиowell Nanoliquid Flow Past Magnetized Riga Device with Nonlinear Thermal Radiation, Fluids. 2021;6:1-22416.
Available:https://doi.org/10.3390/fluids6110416

15. Mishra S, Pal D, Mondal H, Sibanda P. On radiative-magnetoconvective heat and mass transfer of a nanofluid past a non-linear stretching surface with ohmic heating and convective surface boundary condition. Propulsion and Power Research; 2016.
Available:http://dx.doi.org/10.1016/j

16. Mondal H, Mishra SPK, Kundu Sibanda P. Entropy generation of variable viscosity and thermal radiation on magneto nanofluid flow with dusty fluid. J. Appl. Comput. Mech. 2020;6(1):171-182
DOI: 10.22055/JACM.2019.28273.1473

17. Kumar MA, Reddy WD, Rao VS, Goud BS. Thermal radiation impact on MHD heat transfer natural convective nano fluid flow over an impulsively started vertical plate. Case Studies in Thermal Engineering. 2021;24:1-10.

18. Fatunmbi EO, Ramonu OJ, Salawu SO. Analysis of heat transfer phenomenon in hydromagnetic micropolar nanoliquid over a vertical stretching material featuring convective and isothermal heating conditions. Waves in Random and Complex Media; 2023.
DOI: 10.1080/17455030.2023.2173494

19. Thriveni K, Mahanthesh B. Optimization and sensitivity analysis of heat transport of hybrid nanoliquid in an annulus with quadratic Boussinesq approximation and quadratic thermal radiation. Eur. Phys. J. Plus. 2020;135:1–22.

20. Fatunmbi EO, Okoya SS. Quadratic mixed convection stagnation-point flow in hydromagnetic casson nanofluid over a nonlinear stretching sheet with variable thermal conductivity. Defect and Diffusion. 2020;409:95-109.

21. Kameswaran PK, Sibanda P, Partha MK, Murthy PVSN. Thermophoretic and nonlinear convection in a non-darcy porous medium. J. Heat Transf. 2014;136(4):042601.

22. Jha BK, Gwandu BJ. MHD free convection in a vertical slit microchannel with super-hydrophobic slip and temperature jump: Non-linear Boussinesq approximation approach. SN Appl. Sci. 2019;1(6):603.

23. RamReddy C, Naveen P, Srinivasacharya D. Influence of non-linear Boussinesq approximation on natural convective flow of a power-law fluid along an inclined plate under convective thermal boundary condition. Nonlinear Eng. 2019;8(1):94О6.

24. Sajjan K, Shah NA, Ahammad NA, Raju CSK, Kumar MD, Weera W. Nonlinear boussinesq and rosseland approximations on 3D flow in an interruption of ternary nanoparticles with various shapes of densities and conductivity properties. AIMS Mathematics. 2022;7(10): 18416̤8449.
DOI: 10.3934/math.20221014

25. Mahanthesh B, Mackolil J, Radhika M, Al-Kouz W, Siddabasappa M. Significance of quadratic thermal radiation and quadratic convection on boundary layer two-phase flow of a dusty nanoliquid past a vertical plate. International Communications in Heat and Mass Transfer. 2020:105029.
Available:https://doi.org/10.1016/j.icheatmasstransfer

26. Ali ME. Heat transfer characteristics of a continuous stretching surface. Warme-und Stoffubertragung. 1994;29(4):227-234.

27. Attili BS, Syam ML. Efficient shooting method for solving two point boundary value problems. Chaos, Solitons and Fractals. 2008;35(5):895-903.

28. Mahanthesh B, Gireesha BJ, Gorla RSR, Makinde OD. Magnetohydrodynamic three-dimensional flow of nanofluids with slip and thermal radiation over a nonlinear stretching sheet: A numerical study. Neural Computing and Applications. 2018;30(5): 1557-1567.

29. Grubka LJ, Bobba KM. Heat transfer characteristics of a continuous, stretching surface with variable temperature. Heat Transfer. 1985;107:1-3.

_____

Peer-review history:
The peer review history for this paper can be accessed here:
https://www.sdiarticle5.com/review-history/102683